East European Journal of Physics. 3. 466-475 (2025)
DOI:10.26565/2312-4334-2025-3-51 ISSN 2312-4334

A 31% EFFICIENT CIGS-BASED SOLAR CELL USING SPIRO MATERIAL AS A BUFFER LAYER: NUMERICAL SIMULATION

Mohamed Hamdaoui[a]*, Lhoussayne Et-taya[a], Abdellah Benami[a], Malika Ouhadou[a], Abderrahman El Boukili[b], Jaouad Fosh[c]

[a]*Optoélectronique et Techniques Energétiques Appliquées, Department of Engineering Sciences, Faculty of sciences and techniques, Moulay Ismaïl University of Meknès BP 509 Boutalamine, Errachidia, Morocco*
[b]*Physique Moderne, Rayonnement et Applications, Department of Engineering Sciences, Faculty of sciences and techniques, Moulay Ismaïl University of Meknès BP 509 Boutalamine Errachidia, Morocco*
[c]*Électronique et Systèmes Intelligents, Optoelectronics and Applied Energy Technics (OAET), Department of Engineering Sciences, Faculty of sciences and techniques, Moulay Ismaïl University of Meknès BP 509 Boutalamine Errachidia, Morocco*
**Corresponding Author E-mail: m.hamdaoui@umi.ac.ma*
Received March 31, 2025; revised June 26, 2025; accepted July 15, 2025

This study investigates the potential boost of (Cu(In,Ga)Se2) based solar cells through numerical simulations using SCAPS-1D software to optimize their performance. Various parameters were analyzed, including the thickness, acceptor concentration, and band gap of the CIGSe active layer, as well as the donor concentration and thickness of the ZrS_2 buffer layer. The impact of operating temperature was also considered. The optimized output characteristics of the proposed cell design include a V_{OC} of 1.13V, J_{SC} of 32.61mA/cm², FF of 89.12, and a PCE of 32.91. These findings can aid in advancing the development of high-efficiency CIGSe-based thin-film solar cells.
Keywords: *SCAPS; Operating temperature; Thickness; Work function; Parameter of solar cells*
PACS: 42.79.Ek, 78.20.Bh, 72.80.Le, 73.30.y, 73.40.Kp

1. INTRODUCTION

Despite the depletion of fossil resources, the need for energy is growing every year, which is vital for worldwide technological and economic development1. As an environmentally advantageous technology that decreases worldwide CO_2 emissions, solar cells are recognized one of the most important renewable energy sources.

Like a hybrid of organic and inorganic materials, PSCs, or perovskite solar cells, have advanced remarkably during the past ten years; their energy conversion efficiency has improved from 3.8% in 2009 to 25.5% in 2024. An essential factor for generating effective and stable PSCs is the choosing of hole transport layers (HTLs).

As a clean energy source, solar cells are in demand, and copper indium gallium selenide (CIGS) is showing talent [1]. Because of its direct bandgap, A significant optical absorption coefficient is present in CIGS, allowing active materials to use thin layer (1–2 μm) [2]. But as virgin spiro-OMeTAD has limited hole mobility and does not fulfill device performance parameters, chemical doping is necessary to boost its conductivity and, consequently, its hole extraction capacity [3].

First and foremost, the goal of this research is to increase a simple solar cell's efficiency as defined by [4]. As a result, we suggest using an HTL hole transport layer in this study and experimenting with the energy gap and charge carrier concentration to get the best performance. This study investigates how two crucial solar cell characteristics affect the photovoltaic performance of simple CIGS/ZrS_2 devices: The thickness and band gap of the active layer (absorber).

However, to maximize perovskite solar cells' optical and electrical performance, the hole transport layer is an essential component that improves the optoelectronic properties of the cells. Spiro-OMeTAD is widely used as a hole transport material in perovskite solar cells (PSCs). However, the mobility and conductivity of virgin or oxygen-oxidized spiro-OMeTAD are restricted [5]. Cumene hydroperoxide-oxidized spiro-OMeTAD, which has several benefits as an HTL, is used in this study. It is undeniable that the reduction of particle density, the optimization of the perovskite energy-to-layer ratio, and the ease of carrier movement all contribute to improved cellular efficiency.

2. MODELING FRAMEWORK AND MATERIAL PARAMETERS

We utilized a solar cell structure that was derived from the research conducted by [4]. for the purposes of this investigation. Figure 1.a shows the framework that will be used to improve these results, while Figure 1.b shows the suggested framework based on a modified version of the foundational structure that includes a spiro layer. In order to investigate potential methods of improving the device's efficacy, we implemented a sequence of alterations to the cell structure. An innovative addition has been incorporated into our proposed configuration we inserted a HTL the absorbent layer and the contact layer behind by using the SPIRO material (refer to Figure 1.b).

As shown in Table 1, the physical parameters for the different material layers in this work were carefully collected using a mix of theoretical considerations, well-researched literature sources, and careful estimate, it's noted that the thermal velocity of the electron and the hole is established at 1×10^7 cm/s for all layers.

Cite as: M. Hamdaoui, L. Et-taya, A. Benami, M. Ouhadou, A. El Boukili, J. Fosh, East Eur. J. Phys. 3, 466 (2025), https://doi.org/10.26565/2312-4334-2025-3-51

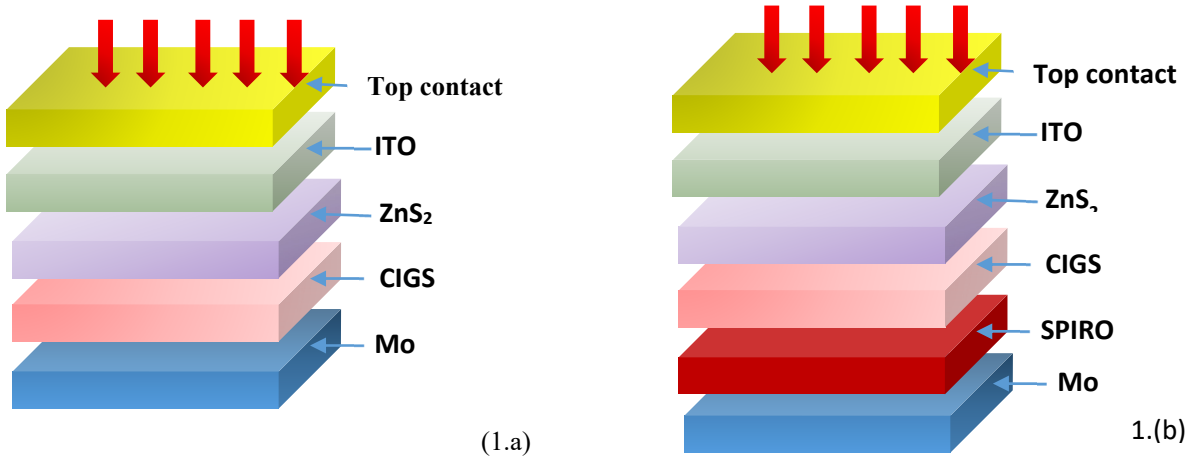

Figure 1. structure of the solar cell without HTL (1.a) and with HTL (1.b).

Table 1. Key material properties that were employed in this simulation

Materials Parameters	ITO [6]	n-ZrS_2 [7]	p-CIGSe [5]	$CuSbS_2$ [8]	P3HT [9]	Cu_2O[9]	Spiro [10, 11]
Bandgap (eV)	3.6	1.5-1.9	1.4	1.58	1.7	2.17	1.6
Thickness (nm)	40	100-400	200-2000	50	50	50	50
Dielectric permittivity	8.9	16,4	13.6	14.6	3	7.2	3
Electron affinity (eV)	4.5	4.7	4.5	4.2	4.5	3.2	4.07
C_B density of states (cm^{-3})	2.2×10^{18}	2.2×10^{18}	2.2×10^{18}	2×10^{18}	2×10^{18}	2.5×10^{20}	2.5×10^{18}
V_B density of states (cm-3)	1.8×10^{19}	1.8×10^{19}	1.8×10^{19}	1×10^{19}	1.8×10^{19}	2.5×10^{20}	2.2×10^{19}
Hole mobility (cm^2/Vs)	10	1300	25	49	1.8×10^{-2}	8600	18
Electron mobility (cm^2/Vs)	10	2300	200	49	1.8×10^{-3}	200	100
Donor density (cm^{-3})	1×10^{18}	1×10^{14}-1×10^{18}	0	1×10^{18}	0	-	0
Acceptor density (cm^{-3})	0	0	1×10^{14}-1×10^{18}	0	1×10^{18}	1×10^{19}	1×10^{18}

2.1. Numerical simulation

Within the framework of our research, we used SCAPS-1D, a digital simulation program known for its sophistication and usefulness in the analysis and comprehension of physical phenomena produced by photovoltaic devices. This tool has enabled us to model and assess our solar cells. The standard test conditions (STC) were implemented in each SCAPS-1D simulation with a luminescence intensity of AM 1.5 (100 mW/cm^2).

The displacement of charge carriers along the superposition axis is described by the solution of the Poisson equations in conjunction with the continuity equations for the electrons and the trous [12].

Solving Poisson's equations in combination with the continuity equations for holes and electrons characterizes the passage of charge carriers down the superposition axis [13].

$$\frac{d^2}{dx^2}\psi(x) = \frac{q}{\varepsilon}[p(x) - n(x) + N_D - N_A + N_t] \quad (1)$$

$$\frac{1}{q}\frac{d}{dx}J_n = R_n(x) - G_{op}(x) \quad (2)$$

$$\frac{1}{q}\frac{d}{dx}J_P = G_{op}(x) - R_n(x) \quad (3)$$

Where;

- ψ denotes the electrostatic potential,
- N_t represents the defect density,
- q signifies the elemental charge, ε indicates permittivity,
- p refers to the concentrations of free electrons,
- n refer to concentrations of holes,
- N_A correspond to the densities of ionized acceptors,
- N_D is to the densities of ionized donors,
- J_n and J_p represent the current densities of electrons and holes,
- G_{op} denote the rates of electron-hole pair generation,
- R_n represent the rates of electron-hole pair recombination.

3. RESULTS AND DISCUSSION

3.1. Optimization of a Conventional Solar Cell

As it's mentioned, as our reference cell for the sake of this investigation, we used a solar cell structure that was motivated by the findings of [5], We implemented a number of modifications to the cell structure in order to investigate possible methods to progress the device's competence.

In this section, we will first examine how the thickness of the absorption layer, the band gap, and density sensors affect the primary photovoltaic characteristics: open circuit tension (Voc), closed circuit current density (Jsc), filling factor (FF), and cell efficiency (η), respectively.

As seen in Figure 2, the photovoltaic cell model used in this simulation study consists of the following components: the metal/metal electrode (HTL), CIGS (perovskite absorption layer), ZnS2 (ETL), and FTO (transparent conductive oxide). Table 1 displays the characteristics established for the solar cell structure in this simulation, such as thickness, band gap, electrical permittivity, electronic affinity, electron/hollow mobility, and thermal electron/hole velocity.

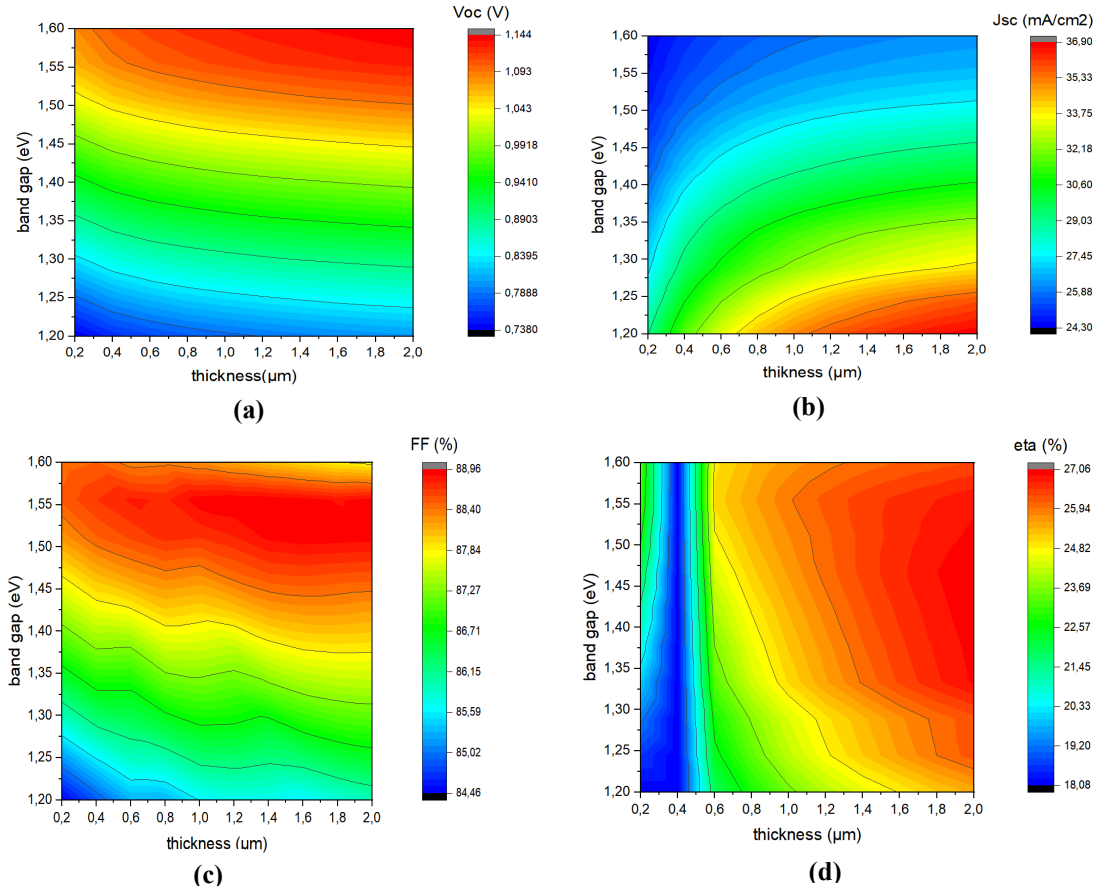

Figure 2. The simulated solar cells basic parameters including Voc (a), Jsc (b), FF (c), and η (d) as function on

This section aims to explain how the photovoltaic performance of the basic CIGS/ZrS_2 structure is impacted by two important solar cell parameters: the thickness and the absorber and tampon cushion band gaps. The thickness and the interdict band were changed from 0.2 to 2.0 µm and 1.2 to 1.6 V, respectively, in the first phase. In the second step, we examine how the thickness of the ZrS_2 couche and its energy difference affect solar cell performance in order to optimize the couche tampon's parameters. The final step is to ascertain how the concentration of donors ZrS_2 and acceptors CIGS (NA) affects the main parameter of the solar cell under study.

3.1.1. Exploring the impact of the CIGC thickness and band gap on conventional solar cell properties

It is commonly recognized that the absorber layer's thickness, band gap, and carrier concentration have a significant impact on how effectively solar cells work. The impact of the CIGS layer's thickness and band gap on solar cell performance was investigated in order to maximize the absorber layer properties.

It is well acknowledged that the properties of the absorbent layer, such as its thickness, band separation, and porteur density, are crucial for optimizing the performance of solar panels [14,15]. We have investigated how the thickness and band gap of the CIGS layer affect the efficiency of solar cells in order to enhance the properties of the absorption layer.

The contour plot depicting the interplay between absorber thickness and band gap energy of the CIGS layer of the basic structure is illustrated in Fig. 2, and how these variables impact the performance metrics of the device. We take a range of thickness from 0.2 to 2 µm and the gap energy from 1.2 to 1.6 eV. It is clear from this figure, that J_{SC} decreases

from about 36.90 mA/cm^2 at Eg of 1.2 eV to about 24.30 mA/cm^2 of 1.6 eV for the thickness greater to 0.8 µm however the variation of the J_{SC} with absorber thickness growth from 0.2 to 2 µm. The Voc and FF decrease when the thickness increases but they rise with the variation of Eg. The efficiency decreases as the thickness of CIGS increases while remaining constant at Eg greater than 1.3eV. The reason for this is that 1.3 eV represents the ideal value for a solar cell, enabling it to absorb the maximum quantity of solar radiation, which in turn leads to the generation of electron-hole pairs and an enhancement of the cell's efficiency [16]. Consequently, research indicates that CIGS serves as the most effective material to minimize usage. The optimal parameters determined for our new cell design are as follows: VOC = 1.06V, JSC = 28.76 mA/cm², FF = 88.55%, η = 27.5%, with a thickness of 2 µm and an energy band gap of 1.46 eV.

Since it has been noted in the literature that device performance declined when Eg approached 1.3 eV, the impact of a larger uniformly variable energy band-gap has not been fully examined [17].

These results may be explained by expanding the interdite band, the local efficacy of the lumineous absorption collection, and the interface between the p-CIGS chopped and n-ZnS_2 films. According to the following equation, this would raise the porteurs' output rate and, as a result, dramatically raise the Voc value [18]:

$$V_{oc} = \frac{k_B T}{q} \ln\left(1 + \frac{I_{ph}}{I_0}\right) \tag{4}$$

In this equation, $k_{B,T}$ and I_{ph} are the Boltzmann constant, the ambient temperature, and the photogenerated current respectively.

Additionally, this said that a clifflike band alignment is thought to enhance the charge separation process based on the CIGS and ZnS2 bandgap values [7].

3.1.2. Exploring the effect of the ZrS_2 thickness and band gap on conventional Solar Cell properties

Having determined the optimal values of the mouthpiece thickness and the band gap of the absorber layer of the basic structure, we are now interested in the influence of these two factors on the performance of the buffer layer. as shown in the following figures.

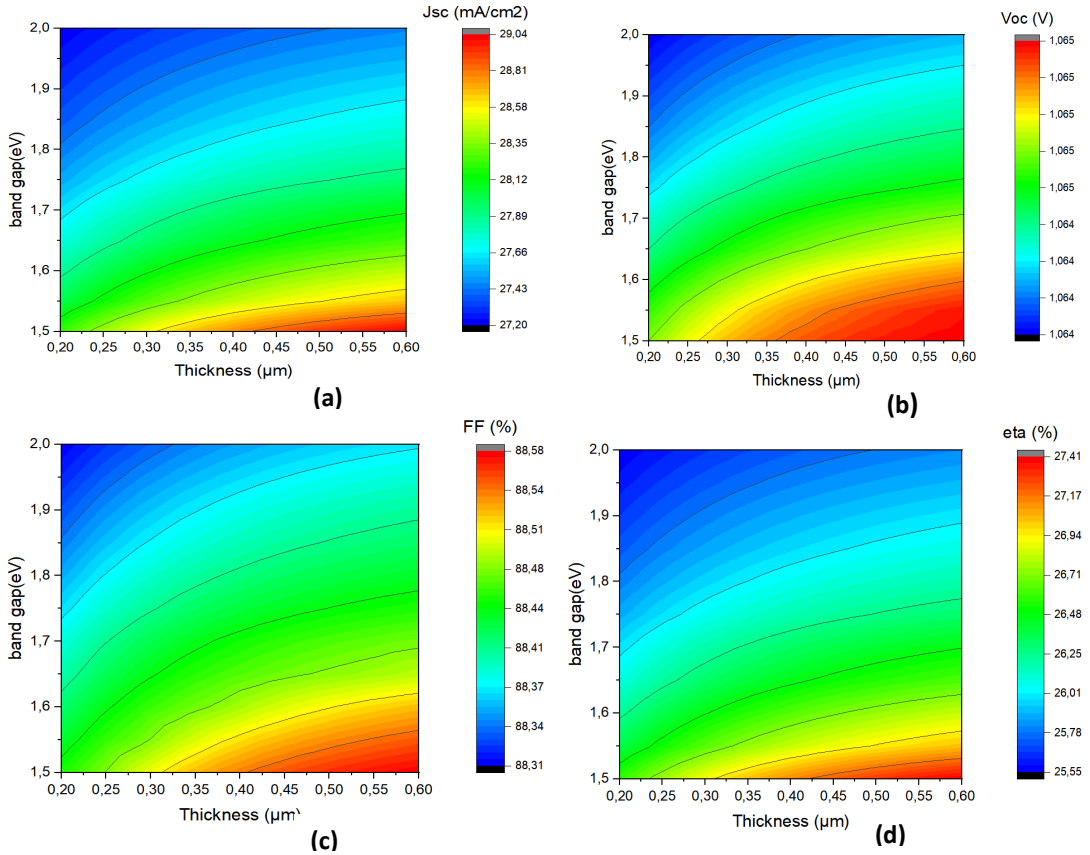

Figure 3. The fundamental parameters of solar cell simulations: Voc (a), Jsc (b), FF (c), and η (d), are displayed according to the thickness of the tampon couch (axis des x) and the concentration of the carriers (axis des y).

Next, we examine how the ZrS_2 buffer layer's thickness and band gap affect the device performance as seen in the contour plot in Figure 3. The ZrS_2 buffer layer's thickness and band gap energy ranges from 0.20 to 0.60 µm and 1.5 to 2 eV, respectively. There is a consistent relationship among the photovoltaic output metrics Voc, Jsc, FF, and efficiency. This suggests that the cell's overall performance increases when the ZrS_2 layer's thickness expands, but they decline with band gap rise. The development of structural flaws at the buffer layer interface might be connected to this phenomenon.

As a result, ZrS_2's strong lattice mismatch strain reduces optical absorption, which might harm solar cells' overall performance [19, 20]. the best performances found are as follows: V_{OC}=1.06V, J_{SC}=29.03mA/m^2, FF= 88.57% and η=27.40% at 0.6μm and 1.5eV of thickness and band energy of ZrS_2 buffer layer, respectively.

3.1.3. Exploring the Impact of CIGS Na and ZrS_2 N_d on conventional solar cell properties

In order to maximize the efficiency of these solar cells with CIGS based, the impact of variations in ZrS_2 porteurs and CIGS couches on the key parameters of the cited structure has been examined. Fig. 4 exhibits the effect of the acceptor (Na) and donor (Nd) carrier concentration of CIGS and ZrS_2, respectively, Na and N_d varied from 10^{12} to 10^{18} cm^{-3}. The V_{OC}, FF, η rise from 0.77 to 1.06 V, from 81.1 to 82.62% and from 19.14% to 27.42 %; when the Na increases. However, when the acceptor concentration of the CIGS layer increases, the Jsc drops from 29.83 to 29mA/cm^2. Because of dominating recombination and the material's increased resistivity, it is harder to capture photo-generated electrons at larger concentrations, which accounts for the slight decrease in Jsc [21, 22]. However, further increasing the donor concentration in the ZrS_2 thin film does not affect the J_{SC} value between 10^{12} and 10^{18} cm^{-3}. increasing N_d of ZrS_2 has no major effect on cell performance.

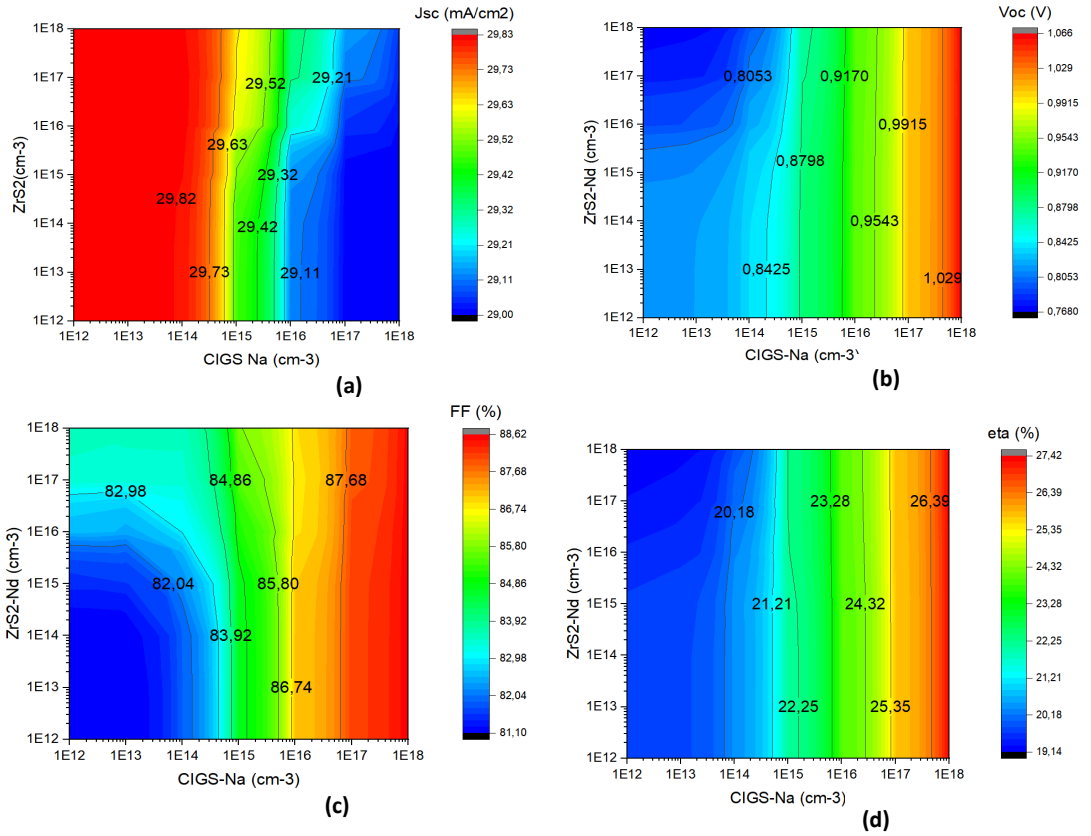

Figure 4. simulated solar cells basic parameters including V_{oc} (a), J_{sc} (b), FF (c), and η (d) as function on CIGS-Na (x-axis) and ZrS_2 Nd (y-axis)

III- Study of solar cell device with HTL material

Spiro-OMeTAD, one of the most widely used hole-transport materials (HTMs) in optoelectronic devices, often requires chemical doping with a lithium compound (LiTFSI) to get sufficient conductivity and efficient hole extraction [23]. Spiro-OMeTAD is a highly researched and effective hole transport layer material (HTL) owing to its ease of application and superior performance in organic-inorganic electronic systems spiro [24]. The spiro-linked molecule offers a high glass transition temperature (Tg), morphological stability, and facile processability, while preserving excellent electrical characteristics.

To indicate the influence of HTL on power conversion efficiency solar cell CIGS based design, the numerical simulations are done and the results are presented. The material properties used for HTL couches are taken from other published works in the literature. Table 1 compiles the essential HTL layer characteristics that were collected from [11, 12] to enhance the solar cell's performance. The impact of altering this layer's band gap on the most crucial solar cell properties using an HTL layer is seen in Figure 5 below. Nutrients improve all of the solar cell's parameters by jointly expanding the hole transport layer's band gap. In detail we notice an improvement in the surface current from 31.46 to 32.61mA/cm^2, from 0.71 to 1.04 V for V_{OC}; We also have a form factor improvement of 80.47 percent to 86.49 % and an efficiency improvement of rom 19.04 to 29.36 % [25].

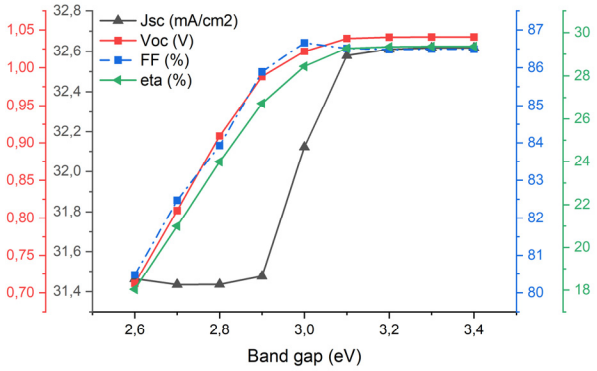

Figure 5. impact of altering the HTL layer's band gap on the solar cell's primary parameters.

It is well known that the band gap affects the mobility of charge carriers (holes) inside the HTL [26]. By facilitating the flow of holes from the active layer to the anode, a suitable band gap can raise the overall efficiency of the solar cell.

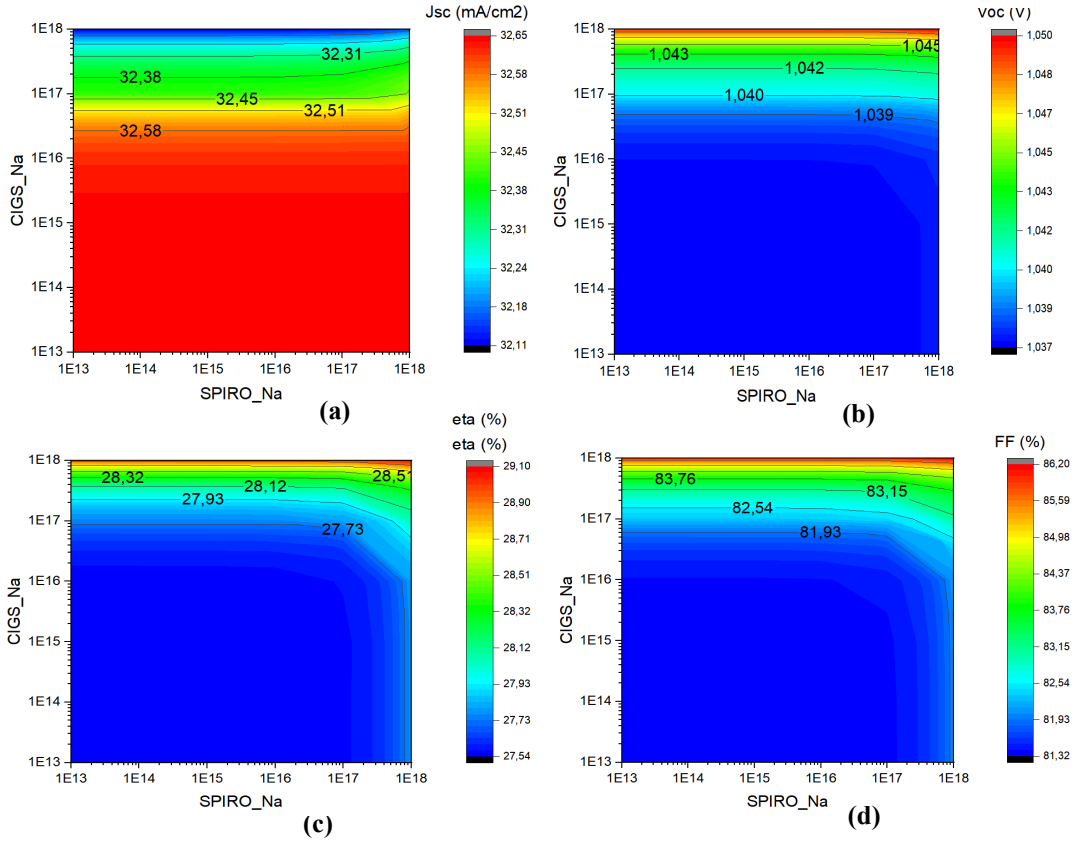

Figure 6. Contour plot of simulated solar cells parameters including Voc, Jsc, FF, and η as function on the Spiro Na (x-axis) and CIGS Na (y-axis)

On the other hand, the alignment of energy levels between the HTL and the active layer (such organic materials or perovskites) is influenced by the band gap. An appropriately matched band gap can promote effective charge transfer and lower interface energy losses [27]. Dance usually we adopted the value 3 eV for the gap because this is the value in which we found the best optimization of the solar cell.

To investigate the effects of acceptor density in the two layers, namely Spiro and CIGS, the following study was carried out, we vary the density of the acceptors for the two layers between an exponential 1.10^{12} and $1.10^{18}/cm^3$. Based on figure 6, we can assume that since all parameters essentially stay the same, changes in the layer's total acceptor density have no consequence on the solar cell's efficiency. The value of Na = $10^{18}/cm^3$ has been set at for the two layers based on the results.

3.2. Operating temperature effects on the efficiency of solar cells

In this paragraph, in Fig. 7, the influence of operating temperature on the fundamental parameters of the basic structure and the optimal CIGS/ZrS_2/Spiro solar cell was explored. The following graphs show how the operational temperature affects two different configuration types: the basic setup without HTL and the suggested design that relies

on SPIRO-MeTAD as a HTL layer. These curves clearly show that the suggested cellule's performance is not much impacted by temperature increases. Which is consistent with other previously published studies. It can be confirmed that the construction exhibits good stability in the face of temperature changes. which states that when temperature rises and the charge carrier recombination probability increases, the opposite saturation current (Io) increases and, therefore, the Voc, Jsc, and η values decrease [28].

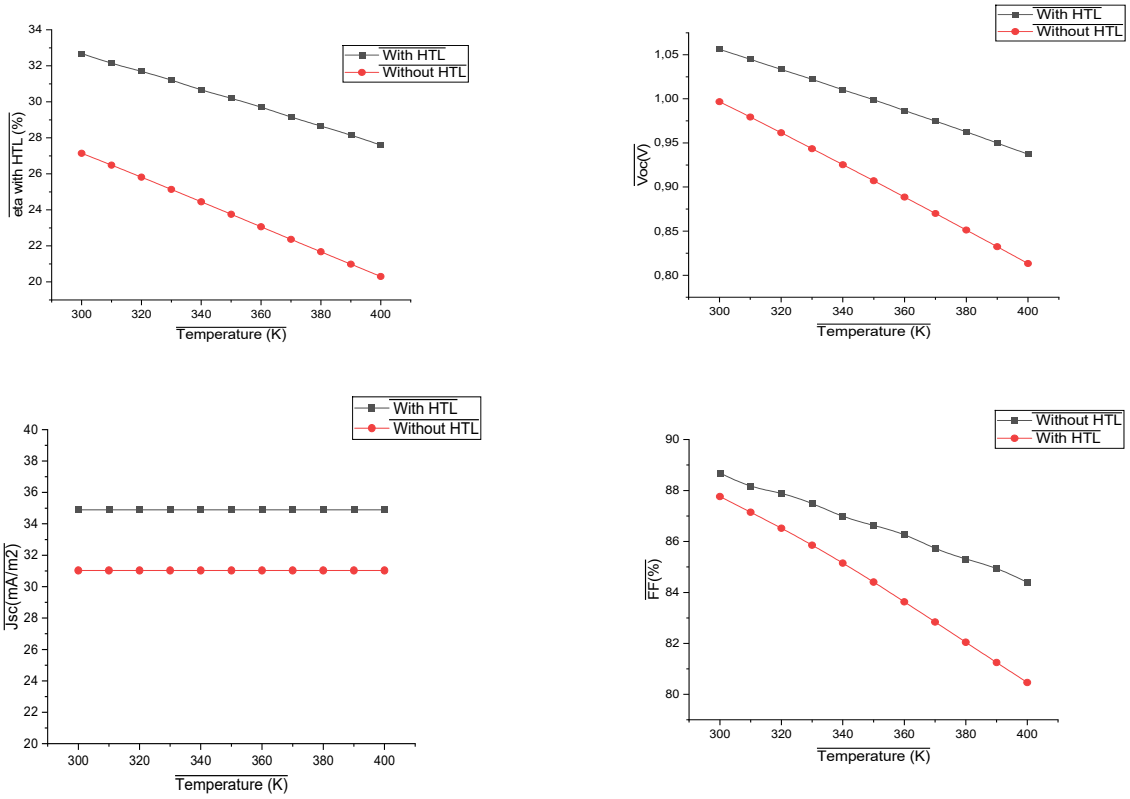

Figure 7. Impacts of the and temperature solar cell performances with and without HTL

4. COMPARATIVE STUDY OF THE PROPOSED STRUCTURE

4.1. Comparative analysis with another HTL layers

In the preceding paragraph, we demonstrated the value of including an HTL sofa into the structure using Spiro MeTAD; nevertheless, it is necessary to test more HTL materials and observe their impact on the building's performance. Consequently, many HTMs (ZrS_2, $CuSbSe_2$, P3HT, Cu_2O and Spiro-OMeTAD) have been used to enhance simulation and guide experimental research in order to justify the use of spiro-OMeTAD as HTL. Table 1 displays the input parameters for the various HTL couches mentioned. The photovoltaic parameters obtained using various devices based on various HTL are shown in Table 2. It's noted that the total defect density (Nt) for each layer is taken for 1.00×10^{14} cm^{-3}.

Table 2. The input characteristics for the various HTL layer mentioned

HTL	Voc(V)	Jsc(mA/cm²)	FF(%)	PCE(%)	Ref
ZrS_2	0.997	31.03	88.00	27.22	[7]
$CuSbS_2$	1.07	32.62	87.35	30.69	[8]
P3HT	1.07	32.60	79.89	28.05	[9]
Cu_2O	1.07	32.59	84.95	29.83	[9]
Spiro	1.02	35.41	87.84	31.71	This work

This configuration of Spiro-HTL-based showed an excellent photovoltaic conversion yield of 31.71%, which was greater than that of other devices based on other HTMs, according to our testing of many HTMs based on the structure proposed in this study. Compared to the ather configurations with HTL, Spiro-OMeTAD-HTL we were able to get higher values for Jsc, FF and PCE. (Jsc=35.41mA/m^2, FF=87,84% and PEC=31.71).

4.2. Comparative study with other works

Using various tampon couches from other works, Table 3 compares the performance of the solar cells under investigation with that of the CIGS solar cells examined in other studies. The data makes it clear that the optimal efficiency we achieved in our research is 26.75%, which compares well with the results of other studies on solar cells CIGS.

An overview of certain published works has been done in order to arrange the solar cellule in such an optimal manner. This course demonstrates that the optimized structure has one of the best configurations at the performance level that touches more than 31.71%.

Table 3. Comparative studies with other works

Cell structur	Voc(V)	Jsc(mA/cm^2)	FF(%)	PCE(%)	Ref
SnO_2/ ZnSe/ CIGS/ / Mo	0.8242	21.08	79.70%,	13.85%	[29]
ZnO/CdS/CIGS/Mo	0.7436	34.47	83.09	21.3	[30]
ITO/ZrS_2/CIGS/Mo	1.0063	30.35	88.24	26.95	[4]
ZnO:Al/ZnO-i/Cd/CIGS /Mo	0.82	43.3	84%,	29.82%,	[31]
ZnO:Al/ZnS2/CIGS/SPIRO/Mo	1.02	35.41	87.84	31.71	This work

4.3. Parameters of the optimal final cell

The following Figure 7 present the four fundamental parameters of the suggested cell output with Spiro as a HTL layer. As can be seen in this figure, the developed cell presents the following values. The most interesting is its exceptional efficiency of 31.7%. Given these considerations, this structure can be an alternative solution for photovoltaic systems.

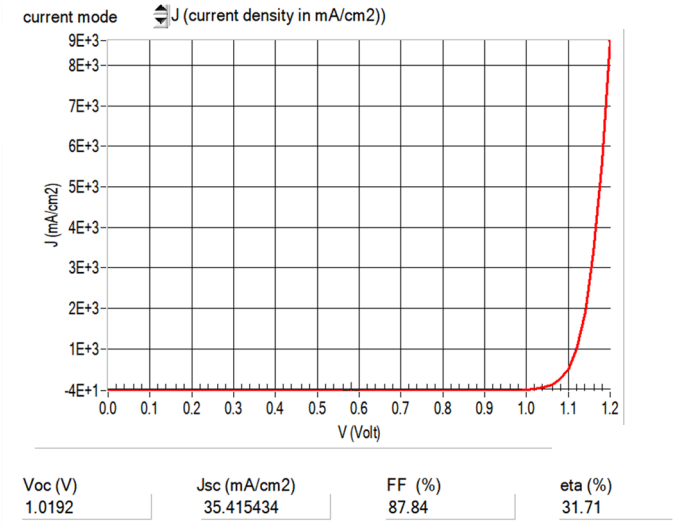

Figure 7. the main parameters of the optimized structure with HTL

5. CONCLUSION

We have utilized the SCAPS-1D software in this work to do numerical simulations and illustrate the potential of solar cells in Cu(In,Ga)Se2 in order to maximize their performance. Among the many fundamental structural characteristics examined were the thickness, acceptor concentration, and band gap of the ZrS_2 tampon couche, as well as the donor concentration and thickness of the CIGSe absorber layer. The performance of the cells was further enhanced in the other section of this study by adding a Spiro as a buffer. Additionally taken into account was the effect of operational temperature. The suggested cell design's optimal output statistics include a PCE of 31.71%, a JSC of 35.41 mA/cm^2, an FF of 87.84%, and a V_{OC} of 1.02 V. These findings might contribute to the advancement of thin-film solar cells based on CIGSe that have excellent efficiency.

ORCID

Mohamed Hamdaoui, https://orcid.org/0009-0008-9063-0984; **Lhoussayne Et-taya,** https://orcid.org/0000-0002-9815-3667
Abdellah Benami, https://orcid.org/0000-0001-5516-5660; **Malika Ouhadou,** https://orcid.org/0000-0002-9751-2381
Abderrahman El Boukili, https://orcid.org/0000-0002-3277-9640; **Jaouad Foshi,** https://orcid.org/0000-0002-8509-6130

REFERENCES

[1] A. Azmand and A.H. Kafashan, "Al-doped ZnS thin films: Physical and electrochemical characterizations," J. Alloys Compd. **779**, 301-313 (2019). https://doi.org/10.1016/j.jallcom.2018.11.268
[2] R.N. Bhattacharya, M.-K. Oh and Y. Kim, "CIGS-based solar cells prepared from electrodeposited precursor films," Sol. Energy Mater. Sol. Cells, **98**, 198–202 (2012). https://doi.org/10.1016/j.solmat.2011.10.026
[3] Qi Chen, et al., "Spiro-OMeTAD doped with cumene hydroperoxide for perovskite solar cells," Electrochemistry Communications, **126**, 107020 (2021). https://doi.org/10.1016/j.elecom.2021.107020
[4] H. Kafashan and A. Bahrami, "CIGS solar cells using ZrS_2 as buffer layer: Numerical simulation," Optik - International Journal for Light and Electron Optics, **298**, 171594 (2024). https://doi.org/10.1016/j.ijleo.2023.171594
[5] P. Ganesan, et al., "A simple spiro-type hole transporting material for efficient perovskite solar cells," Energy. Environ. Sci. **8**(7), 1986–1991 (2015). https://doi.org/10.1039/C4EE03773A

[6] M. Al-Hattab, et al., "Numerical simulation of a new heterostructure CIGS/GaSe solar cell system using SCAPS-1D software," Sol. Energy, **227**, 13–22 (2021). https://doi.org/10.1016/j.solener.2021.08.084
[7] M. Moustafa, T. Al Zoubi and S. Yasin, "Exploration of CZTS-based solar using the ZrS_2 as a novel buffer layer by SCAPS simulation," Opt. Mater. **124**, 112001 (2022). https://doi.org/10.1016/j.optmat.2022.112001
[8] M. Ameri, E. Mohajerani, M. Ghafarkani, N. Safari and S.A. Alavi, "The investigation of the unseen interrelationship of grain size, ionic defects, device physics and performance of perovskite solar cells," J. Phys. D Appl. Phys. **52**, 125501 (2019). https://doi.org/10.1088/1361-6463/AAFEA9
[9] Y. Raoui, H. Ez-Zahraouy, N. Tahiri, O. El Bounagui, S. Ahmad and S. Kazim, "Performance analysis of MAPbI (3) based perovskite solar cells employing diverse charge selective contacts: Simulation study," Sol. Energy, **193**, 948–955 (2019). https://doi.org/10.1016/j.solener.2019.10.009
[10] S. Karthick, J. Boucle and S. Velumani, "Effect of bismuth iodide (BiI_3) interfacial layer with different HTL's in FAPI based perovskite solar cell-SCAPS-1D study," Sol. Energy, **218**, 157–168 (2021). https://doi.org/10.1016/j.solener.2021.02.041
[11] A. Hima, N. Lakhdar and A. Saadoune, "Effect of Electron Transporting Layer on Power Conversion Efficiency of Perovskite-Based Solar Cell: Comparative Study," Journal of Nano- and Electronic Physics, **11**, 01026 (2019). https://doi.org/10.21272/jnep.11(1).01026
[12] D. Valencia, J. Conde, A. Ashok, C.A. Meza-Avendaño, H. Vilchis and S. Velumani, "Optimization of Cu(In, Ga)Se2 (CIGSe) thin film solar cells parameters through numerical simulationand experimental study," Sol. Energy, **224**, 298-308 (2021). https://doi.org/10.1016/j.solener.2021.05.075
[13] H. Aissat, H. Arbouz and J.P. Vilcot, "Optimization and improvement of a front graded bandgap CuInGaSe2 solar cell,", Solar Energy Materials and Solar Cells, **180**, 381-385 (2018). https://doi.org/10.1016/j.solmat.2017.09.017
[14] A. Belghachi and N. Limam, "Effect of the absorber layer band-gap on CIGS solar cell," Chinese Journal of Physics, **55**(4), 1127-1134 (2017). https://doi.org/10.1016/j.cjph.2017.01.011
[15] S. Bechlaghem, B. Zebentout and Z. Benamara, "The major influence of the conduction-bandoffset on Zn (O, S)/CuIn0.7Ga0.3Se2 solar cells," Results in Physics, **10**, 650-654 (2018). https://doi.org/10.1016/j.rinp.2018.07.006
[16] L. Et-taya, T. Ouslimane and A. Benami, "'Numerical Simulation of Third-Generation Solar Cells Based on Kesterite CZTSSe Using SCAPS-1D," in: *Proceedings of the 3rd International Conference on Electronic Engineering and Renewable Energy Systems. ICEERE*, 2022. Lecture Notes in Electrical Engineering, editet by H. Bekkay, A. Mellit, A. Gagliano, A. Rabhi, and A. Koulali, vol. **954**. (Springer, Singapore, 2022). http://dx.doi.org/10.1007/978-981-19-6223-3_31
[17] Y. Osman, M. Fedawy, M. Abaza and M.H. Aly, "Optimized CIGS based solar cell towards an efficient solar cell: impact of layers thickness and doping", Optical and Quantum Electronics, **53**, 245 (2021). https://doi.org/10.1007/s11082-021-02873-4
[18] M. Abdelfatah, et al., "Fabrication and characterization of low cost Cu_2O/ZnO: Al solar cells for sustainable photovoltaics with earth abundant materials," Sol. Energy Mater. Sol. Cells, **145**, 454–461 (2016). https://doi.org/10.1016/j.solmat.2015.11.015
[19] H. Kafashan and A. Bahrami, "CIGS solar cells using ZrS_2 as buffer layer: Numerical simulation," Optik, **298**, 71594 (2024). https://doi.org/10.1016/j.ijleo.2023.171594
[20] T. AlZoubi and M. Moustafa, "Numerical optimization of absorber and CdS buffer layers in CIGS solar cells using SCAPS," International Journal of Smart Grid and Clean Energy, **8**, 291-298 (2019). https://doi.org/10.12720/sgce.8.3.291-298
[21] L. Et-Taya, A. El Khalfi, M. Ouhadou, A. El Boukili, Md.F. Rahman and A. Benami, "Design and simulation of a new kesterite solar cell structure with and without a perovskite back surface field layer to exceed 32% efficiency," Physica Scripta, **99**(5), 055922 (2024). https://doi.org/10.1088/1402-4896/ad3684
[22] L Et-taya, T. Ouslimane and A. Benami, "Numerical analysis of earth-abundant Cu2ZnSn(SxSe1-x)4 solar cells based on Spectroscopic Ellipsometry results by using SCAPS-1D," Solar Energy, **201**, 827-835 (2020). https://doi.org/10.1016/j.solener.2020.03.070
[23] X. Liu, B. Zheng, L. Shi, et al., « Perovskite solar cells based on spiro-OMeTAD stabilized with an alkylthiol additive," Nat. Photon. **17**, 96–105 (2023). https://doi.org/10.1038/s41566-022-01111-x
[24] C. Lin, G. Liu, X. Xi, L. Wang, Q. Wang, Q. Sun, M. Li, et al., "The Investigation of the Influence of a Cu2O Buffer Layer on Hole Transport Layers in MAPbI3-Based Perovskite Solar Cells," Materials, **15**, 8142 (2022). https://doi.org/10.3390/ma15228142
[25] S. Rabhi, et al., "The impact of CBz-PAI interlayer in various HTL-based flexible perovskite solar cells: A drift-diffusion numerical study", Heliyon, **10**(10), e31138 (2024). https://doi.org/10.1016/j.heliyon.2024.e31138
[26] H.S. Najafabadi, M.A. Meier and G.A. Hallock, "Charge carrier transport and electrical response by driving band gap modulation in semiconductors," Applied Materials Today, **29**, 101608 (2022). https://doi.org/10.1016/j.apmt.2022.101608
[27] L.V.T. Merino, et al., "Impact of the valence band energy alignment at the hole-collecting interface on the photostability of wide band-gap perovskite solar cells", Joule, **8**(9), 2585-2606 (2024). https://doi.org/10.1016/j.joule.2024.06.017
[28] A. Chen and K. Zhu, "Computer simulation of a-Si/c-Si heterojunction solar cell with high conversion efficiency,". Sol. Energy, **86**, 393–397 (2012). https://doi.org/10.1016/j.solener.2011.10.015
[29] Rihana, S.F. Ahmed and M. Khalid, "Simulation of CIGS based solar cells with SnO2 window layer using SCAPS-1D," in: *2019 International Conference on Power Electronics, Control and Automation (ICPECA)*, (New Delhi, India, 2019), pp. 1-4. https://doi.org/10.1109/ICPECA47973.2019.8975461
[30] H. Heriche, Z. Rouabah and N. Bouarissa, "New ultra-thin CIGS structure solar cells using SCAPS simulation program," International Journal of Hydrogen Energy. **42**, 9524-9532 (2017). https://doi.org/10.1016/j.ijhydene.2017.02.099
[31] M. Hamdaoui, L. Et-Taya, J. Foshi, N. Mansour and A. Benami, "Enhancement of the performance of solar cells based-CIGSe by using SCAPS-1D," in: *2024 International Conference on Circuit, Systems and Communication (ICCSC)*, (Fes, Morocco, 2024), pp. 1-4, https://doi.org/10.1109/ICCSC62074.2024.10617204

СОНЯЧНІ ЕЛЕМЕНТИ З 31% ЕФЕКТИВНІСТЮ НА ОСНОВІ CIGS З ВИКОРИСТАННЯМ МАТЕРІАЛУ SPIRO ЯК БУФЕРНОГО ШАРУ: ЧИСЕЛЬНЕ МОДЕЛЮВАННЯ

Мохамед Хамдауї[a], Луссейн Ет-Тая[a], Абделла Бенамі[a], Маліка Ухаду[a], Абдеррахман Ель Букілі[b], Джауад Фош[c]

[a]Департамент інженерних наук, оптоелектроніка та прикладні енергетичні методи, факультет наук і техніки, університет Мулая Ісмаїла в Мекнесе BP 509 Буталамін, Еррачідія, Марокко

[b]Кафедра інженерних наук, сучасна фізика, радіація та застосування, факультет науки і технологій, університет Мулай Ісмаїла в Мекнесі BP 509 Буталамін, Еррашидія, Марокко

[c]Департамент інженерних наук, електроніка та інтелектуальні системи, оптоелектроніка та прикладна енергетика (OAET), факультет наук і техніки, університет Мулай Ісмаїл у Мекнесі, BP 509, Буталамін, Еррашідія, Марокко

У цьому дослідженні вивчається потенційне підвищення потужності сонячних елементів на основі (Cu(In,Ga)Se2) за допомогою числового моделювання з використанням програмного забезпечення SCAPS-1D для оптимізації їхньої продуктивності. Були проаналізовані різні параметри, включаючи товщину, концентрацію акцепторів та ширину забороненої зони активного шару CIGSe, а також концентрацію донорів та товщину буферного шару ZrS_2. Також було враховано вплив робочої температури. Оптимізовані вихідні характеристики запропонованої конструкції елемента включають летючу органічну формулу (VOC) 1,13 В, струм опромінення (JSC) 32,61 мА/см², коефіцієнт деградації (FF) 89,12 та коефіцієнт виходу (PCE) 32,91. Ці результати можуть допомогти у розробці високоефективних тонкоплівкових сонячних елементів на основі CIGSe.

Ключові слова: *SCAPS; робоча температура; товщина; робота виходу; параметри сонячних елементів*